Hindawi
International Journal of Energy Research
Volume 2023, Article ID 9844833, 11 pages
https://doi.org/10.1155/2023/9844833

Research Article

Anodic Reaction in Syngas-Fueled Proton-Conducting Solid Oxide Fuel Cells

Hyun Ho Shin, Junil Choi, Taiho Park, and Won Bae Kim

Department of Chemical Engineering, Pohang University of Science and Technology (POSTECH), 77 Cheongam-Ro, Nam-Gu, Pohang 37673, Republic of Korea

Correspondence should be addressed to Taiho Park; taihopark@postech.ac.kr and Won Bae Kim; kimwb@postech.ac.kr

Received 13 September 2022; Revised 27 November 2022; Accepted 30 November 2022; Published 3 February 2023

Academic Editor: Juan M. Coronado

Anode-supported proton-conducting solid oxide fuel cells (PC-SOFCs) fabricated with two representative proton-conducting oxides, $BaCe_{0.7}Zr_{0.1}Y_{0.1}Yb_{0.1}O_{3-\delta}$ (BCZYYb) and $BaZr_{0.8}Y_{0.2}O_{3-\delta}$ (BZY), were compared to obtain the insight into the electrochemical performances when fueled with syngas at 700°C and the correlation between the anode thickness (0.4, 0.8, and 1.6 mm) and operational stability. We have demonstrated that, in stability tests, the BCZYYb cells exhibited significantly higher maximum power density (MPD) than the BZY cells when operating on H_2, 1.22 and 0.48 W/cm^2 for the BCZYYb and BZY cells, but the BCZYYb cells degraded more rapidly than the BZY cells when operating on syngas. In addition, decreasing the anode thickness significantly enhanced the stability of BCZYYb cells operating on syngas, a reduction of 81, 76, and 71% in MPD for 1.6, 0.8, and 0.4 mm anode after 30 min. The electrochemical impedance spectra and X-ray diffraction patterns indicated that the rapid degradation of cerate-based cells with syngas could be mainly attributed to the considerable increase in polarization resistance due to the phase decomposition of the electrolyte powder in the anode. Heterogeneous catalysis was performed to study the catalytic reaction of the H_2–CO mixture over anode powders prepared with the two proton-conducting oxides (Ni-BCZYYb and Ni-BZY) in a fixed bed reactor, and the CO conversion and selectivity to CO_2 and CH_4 were determined. For all anode powders, continuous CO_2 production was initially observed with CH_4 formation, and no significant difference in catalytic activity trends was observed between both anode powders. An increased residence time substantially decreased the normalized CO_2 yield, which was associated with the potential secondary reaction of CO_2 with H_2, CH_4, or perovskite oxide. Based on the results of heterogeneous catalysis with both anode powders, the observed cell degradation on both cells during operation with syngas may be primarily attributed to carbon coking due to CO disproportionation; however, more than 4 times rapid degradation of the cerate-based cell when operating with syngas was clearly demonstrated to be attributed to the decomposition of the electrolyte powder in anode by the resulting CO_2 from the catalytic reaction of the H_2–CO mixture.

1. Introduction

Among various fuel cell technologies, solid oxide fuel cells (SOFCs) have attracted increasing interest as alternative energy generators because of their high efficiency. They generate electrical energy through the direct conversion of chemical energy, so they can run with no pollutant emissions and have excellent fuel flexibility [1, 2]. SOFCs are distinguished by the fact that O^{2-} anions are transported from the cathode to the anode through a dense electrolyte such as yttria-stabilized zirconia, which theoretically allows them to operate with any combustible fuel such as hydrocarbons [3]. However, the high activation energy for the transport of O^{2-} anions inevitably requires an undesirable high operating temperature (>800°C), which increases costs and results in challenges with material incompatibility because of the significant mismatch in thermal expansion coefficients and interdiffusion reactions between cell components [4].

An alternative to lowering the operating temperature is to utilize solid-state proton conductors with lower activation energy (0.4–0.6 eV) for proton transport, which would enable superior electrochemical performance owing to the

high ionic conductivity in the target temperature range of 500–700°C. In contrast to O^{2-} ions, the transport direction of the mobile ions would enhance fuel utilization through water formation at the oxygen electrode and thus minimize fuel dilution [5, 6]. Promising candidates for ceramic proton conductors include perovskite-structure alkaline earth cerates with high conductivity and more chemically stable zirconates in the presence of CO_2 and H_2O. Many researchers have devoted significant effort to optimizing the stoichiometry for stability and conductivity by making a solid solution between cerates and zirconates and using cation substitution [7, 8]. However, despite their potential, the practical application of proton-conducting SOFCs (PC-SOFCs) has lagged behind that of their traditional O^{2-} anion-conducting counterparts because of fabrication challenges originating from poor sinterability and chemical instability. Recently, Duan et al. provided an essential step toward resolving such fabrication challenges through solid-state reactive sintering; they realized the direct conversion of a raw precursor oxide by using a sintering agent such as nickel oxide to fabricate a complete anode-supported SOFC with minimal ohmic loss in a single sintering step [8].

Despite significant advances in terms of material and fabrication, the requirement of hydrogen as the fuel remains one of the biggest challenges for practical implementation of current SOFCs because of the vulnerability of conventional Ni-based anodes to carbon coking and sulfur poisoning [9]. Moreover, switching to a proton transport mechanism would unfortunately induce a potential loss of fuel flexibility because of the absence of an available oxidant on the anode side, which would more likely catalyze carbon coking [3]. Despite the difficulty of directly utilizing hydrocarbons as a fuel for PC-SOFCs, Duan et al. reported that a $BaZr_{0.8}Y_{0.2}O_{3-\delta}$- (BZY-) based single cell performed exceptionally with various hydrocarbon fuel streams and without any modifications to the cell composition or architecture. However, most of the fuel cell tests were conducted at a significantly high inlet steam-to-carbon ratio. As a promising alternative to the vulnerability of conventional Ni-based anodes for hydrocarbon-fueled PC-SOFC, perovskite oxide such as $La_{0.5}Sr_{0.5}Fe_{0.9}Mo_{0.1}O_{3-\delta}$ [10] and $Sr_2Fe_{1.5}Mo_{0.5}O_{6-\delta}$ [11], furthermore, in situ exsolved metallic nanoparticle-structured perovskite such as $Sr_2Fe_{1.4}Ni_{0.1}Mo_{0.5}O_{6-\delta}$ [11] and $Sr_2Fe_{1.4}Co_{0.1}Mo_{0.5}O_{6-\delta}$ [12] which has been extensively studied due to their enhanced structural stability and flexible mixed conductivity, while their application to anode-supported cell structure remains a challenge to be solved.

One approach to realizing PC-SOFCs fueled by hydrocarbons that has recently gained interest has been the hydrocarbon reforming process, which produces synthetic gas (syngas) including H_2 and CO by either steam [13] or CO_2 [10, 14]. This process is shown below:

$$CH_4 + H_2O \longrightarrow CO + 3H_2 \quad (1)$$

$$CH_4 + CO_2 \longrightarrow 2CO + 2H_2 \quad (2)$$

The reforming process offers economic and environmental advantages such as the direct conversion of major greenhouse gases (e.g., CH_4 and CO_2) to hydrogen fuel and syngas, which are key feedstocks for chemical synthesis. Furthermore, the reforming process is potentially applicable to limiting greenhouse gas emissions and eventually realizing a net-zero emission energy system [15]. To pair the reforming process with SOFC technology, one approach has been to integrate an additional catalytic layer with high activity and coking resistance for the reforming process on a conventional Ni-based anode. The resulting H_2 fuel is then electrochemically oxidized to generate electrical power. This approach can potentially minimize the vulnerability of the electrolyte (e.g., doped $BaCeO_3$ perovskite) in the atmosphere, which has high concentrations of CO_2 and water [13]. Combining the reforming process with SOFC technology also offers other significant advantages, such as energy compensation between the extremely endothermic nature of the reforming process and exothermic nature of electrochemical oxidation [16].

Because of the potential advantages of combining SOFC technology with the reforming process, many studies have been focused on developing catalysts for the on-cell reforming process of direct hydrocarbon PC-SOFCs [13, 17]. However, relatively little is known about the durability of conventional cermet anodes against carbon coking or decomposition of the PC oxide by products of unfavorable side reactions between CO and/or H_2 over Ni, such as CO methanation or disproportionation. Furthermore, the extent of the catalytic reaction of the resulting syngas in the microporous anode and how the reaction products affect the electrochemical performance of the anode are still unclear [18, 19].

In this study, high-performance anode-supported PC-SOFCs were fabricated with varying anode thicknesses and using two representative PC oxides: $BaCe_{0.7}Zr_{0.1}Y_{0.1}Yb_{0.1}O_{3-\delta}$ (BCZYYb) and BZY. The objective was to study how the reaction products of the $CO+H_2$ mixture catalyzed over the microporous cermet anode and the residence time would influence the electrochemical performance when fueled by syngas at 700°C. The catalytic reaction of the $CO+H_2$ mixture over PC anode powder samples was observed to clarify the reaction products and mechanism. In addition to measurements of the CO conversion and the selectivity to CH_4 and CO_2, the catalytic reaction was with different residence times to elucidate the potential secondary reaction mechanism from the product CO_2 with other gas-phase products or the PC oxide.

2. Experimental

2.1. Materials and Characterization. Precursor powders were prepared by mixing precise amounts of $BaCO_3$ (>99%, Sigma-Aldrich), CeO_2 (>99%, Sigma-Aldrich), ZrO_2 (>99%, Sigma-Aldrich), Y_2O_3 (>99%, Sigma-Aldrich), Yb_2O_3 (>99%, Sigma-Aldrich), NiO (>99%, Kojundo), and starch (Alfa Aesar) as the pore former to realize the desired stoichiometry for different components. For example, NiO, electrolyte, and starch were mixed at a weight ratio of 48 : 32 : 20 to realize the anode composite. The precursor powder mixture was prepared by planetary ball milling (Retsch, PM100) in ethanol at 400 rpm for 1 h and then was dried. The same

procedure was used to prepare the anode functional layer (AFL) and electrolyte precursor powders by mixing electrolyte and NiO at the weight ratios of 60 : 40 and 99 : 1, respectively, in the absence of starch. X-ray diffraction (XRD) (D8 Advance (Bruker)) with Rigaku Ultima IV was used to analyze the composite anode powders under the conditions of 40 kV and 20 mA in the 2θ range of 20–80°.

2.2. Cell Fabrication. Anode-supported half-cells with a configuration of composite anode support/AFL/electrolyte were fabricated by a single reduced-temperature firing based on solid-state reactive sintering and the drop-coating method. NiO was utilized as a sintering aid for full densification of the electrolyte. Two electrolyte powders were utilized to study their influence in the composite anode on the operation with syngas: BCZYYb and BZY. The anode disc was fabricated by mechanical powder pressing with varying amounts of the prepared anode powders to obtain cells with different anode thicknesses. This was to adjust the residence time of the reactant in the microporous anode. A thin AFL and electrolyte layer were applied on the pressed composite anode pellet by the drop-coating technique. Slurries for the drop coating were prepared by dispersion of the mixed powders in the organic solvent at a fluid-to-solid weight ratio of 10 : 1. The organic solvent comprises a mixture of ethanol and organic binder (V006 (Heraeus)) at a weight ratio of 10 : 0.2. The prepared slurries were mixed by planetary ball milling (Retsch, PM100) for 1 h, which was followed by ultrasonic treatment for 1 h to realize homogeneous dispersion of the powder in the slurry. The well-dispersed AFL slurry was drop-coated onto the composite anode pellet, which was followed by heat treatment at 500°C for 1 h. The same procedure was used to deposit the electrolyte on the coated AFL; then, sintering was carried out at 1400°C for 10 h (1450°C for BZY). The resulting anode thicknesses were characterized using scanning electron microscopy (SEM, Hitachi, S-4300). The paste for the cathode comprised $PrBa_{0.5}Sr_{0.5}Co_{1.5}Fe_{0.5}O_{3-\delta}$ (PBSCF, Kceracell) and the organic binder V006 (Heraeus) at a weight ratio of 1 : 1. The paste was screen-printed onto the electrolyte, and the complete cell was then sintered at 900°C for 4 h. The active area of the cathode was 0.28 cm^2 with a thickness of ~20 μm. The current collector was fabricated from Ag conductive paste (Alfa Aesar) and wire. The anode thickness of the fabricated cell has been characterized by SEM.

2.3. Fuel Cell Testing. The fabricated single cells were mounted on an alumina tube and sealed with an alumina-based ceramic adhesive (552-VFG, Aremco) to fix the cell and prevent gas leakage. The composite anode was reduced under dry H_2 at 700°C before electrochemical measurement, where 200 mL/min dry air was supplied to the cathode as the oxidant, and 50 mL/min dry hydrogen was supplied to the anode as the fuel. The AC electrochemical impedance spectra (EIS) and current–voltage characteristics were collected by using a potentiostat (BioLogic SP-300) at an operating temperature of 700°C in H_2, H_2–N_2, or H_2–CO (molar ratio of mixed gases was 1 : 1) flowing at 50 mL/min. The AC EIS was measured in the frequency range of 250 kHz to 0.1 Hz with a perturbation AC amplitude of 10 mV and under the open-circuit voltage (OCV) condition.

2.4. Catalyst Testing. The catalytic reaction of the CO+H_2 mixture was conducted by using a composite anode powder (Ni-BCZYYb or Ni-BZY at a weight ratio of 6 : 4) as a fixed bed in a continuous-flow quartz tube reactor to evaluate the catalytic activity. Prior to catalyst testing, the anode powders were calcined at 1400°C for 1 h. Then, sieved powder (106–150 μm) was utilized to measure the activity at 700°C after reduction in H_2 for 1 h. The powder sample was kept at the center of the quartz tube reactor by using quartz wool. Reactants (i.e., 1 : 1 mixture of CO and H_2) were fed to the quartz tube reactor at a flow rate of 50 mL/min. The sample size was varied from 0.2 to 1 g to study the influence of the residence time. The concentrations of reactants and products were analyzed for 2 h by using an online gas chromatograph (GC, Agilent 7890) with a 60/80 Carboxen 1000 column and thermal conductivity detector (TCD).

3. Results and Discussion

Single cells were fabricated with two different PC oxides: BCZYYb (0.4 mm thick anode) and BZY (1.6 mm thick anode). They were then tested under various anodic conditions to examine the potentially adverse effect of non-H_2 diluents such as N_2 and CO. Figure 1 shows the V–I characteristics for the fabricated anode-supported cells to compare the electrochemical performances when fueled with H_2, H_2 diluted with N_2 to confirm the dilution effect, and syngas including H_2+CO (molar ratios of the mixed gases were 1 : 1) at 700°C. When H_2 was the fuel, the OCV was 0.94 and 0.935 V for BCZYYb and BZY, respectively, which indicate completely densified electrolytes. This confirms that the 1 wt% NiO sintering aid had no significant effect on the electronic conductivity within the electrolyte under fuel cell conditions [20]. The corresponding maximum power densities (MPDs) of 1.22 and 0.48 W/cm^2 for the BCZYYb and BZY cells, respectively, demonstrate the superior performance of the cells fabricated with PC oxide. When the H_2 fuel was diluted with N_2, the general trends were similar for both the BCZYYb and BZY cells: no significant change in OCV (0.94 and 0.92 V, respectively) and a slight decrease in the MPD (1.19 and 0.46 W/cm^2, respectively). With syngas, the BCZYYb cells exhibited an identical OCV to that with the other fuel streams (0.94 V) while the BZY cells exhibited a slight decrease in the OCV (0.9 V). For the MPD, the BZY cells exhibited a small decrease of 9% compared with that of H_2 diluted with N_2 (0.42 W/cm^2). In contrast, a more substantial decrease of 25% was observed for the BCZYYb cells (0.9 W/cm^2). For the PC-SOFCs, the identical binary diffusivities when H_2 was diluted with N_2 and CO, respectively, imply that the fuel mass transport had a limited effect on the electrochemical performance of PC-SOFCs [21].

The EIS results were used to evaluate the differences in electrochemical performance between the two cells under various anodic conditions. Because the feed stream on the cathode side was kept the same, the observed changes in electrochemical performance may be attributed solely to

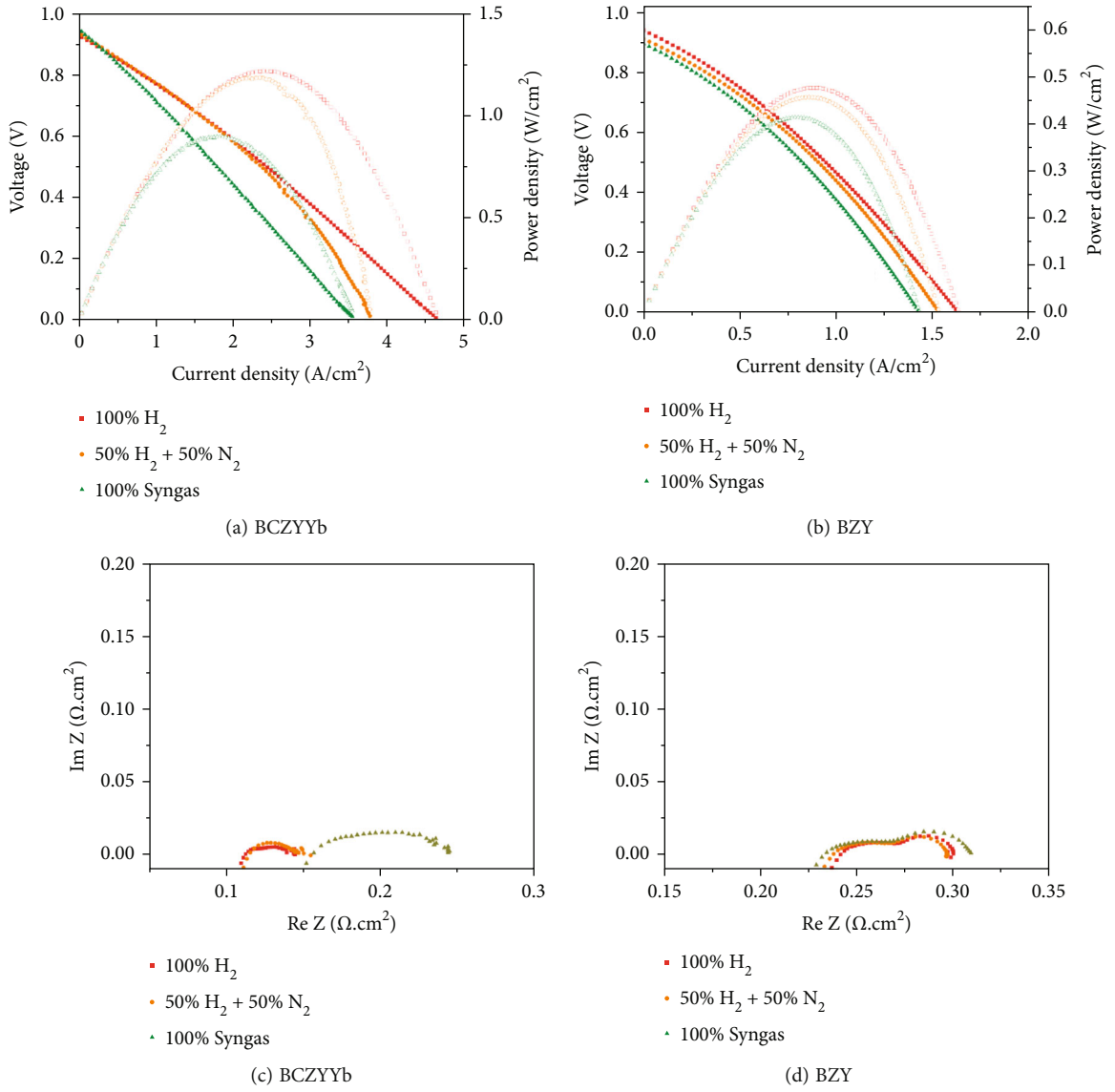

Figure 1: Electrochemical performances of BCZYYb and BZY SOFCs with 0.4 and 1.6 mm thick anodes, respectively, under various anodic conditions (100% H_2, 50% H_2+50% N_2, and 100% syngas): (a, b) I–V–P curves and (c, d) Nyquist plot of the cell performance for BCZYYb and BZY SOFCs at OCV and 700°C.

the changes in anodic conditions. Thus, the effects of N_2 and CO on the anode side on the electrochemical performance were characterized by the EIS for each fuel stream. Figures 1(c) and 1(d) show Nyquist plots of the EIS collected at the OCV under various anodic conditions. The electrolyte ohmic resistance (R_o) was determined from the high-frequency intercept and was 0.11 and 0.24Ω·cm^2 for BCZYYb and BZY, respectively, with the H_2 feed stream. The polarization resistance (R_p) was the span of the impedance arc and indicated the resistance originating from the electrochemical kinetics on the electrodes. R_p was 0.03 and 0.06 Ω·cm^2 for the BCZYYb and BZY cells, respectively, with the H_2 feed stream. The smaller R_p for the BCZYYb cells indicates enhanced electrode kinetics. Despite the corresponding electrolyte thickness and cermet anode composition containing 60 wt% Ni, the smaller R_o and R_p for BCZYYb compared to BZY can be attributed to its higher ionic conductivity, which support a substantially higher maximum current density and power density. Dilution of the H_2 feed stream with N_2 resulted in no significant changes in EIS for both cells at the OCV. The BCZYYb and BZY cells had R_p of 0.04 and 0.058Ω·cm^2, respectively, and R_o of 0.11 and 0.24 Ω·cm^2, respectively. The slight decrease in power density when H_2 was diluted with N_2 may be attributed to anodic concentration polarization due to the higher molecular weight of N_2 [21]. When syngas was the fuel, noticeably, different trends in the EIS were observed for the two cells. For the BCZYYb cells, R_o and R_p increased significantly to 0.15 and 0.08Ω·cm^2, respectively. In contrast, the BZY cells exhibited much smaller increases compared to the other fuels with R_o and R_p of 0.32 and 0.075 Ω·cm^2, respectively. These observations imply that the physicochemical properties

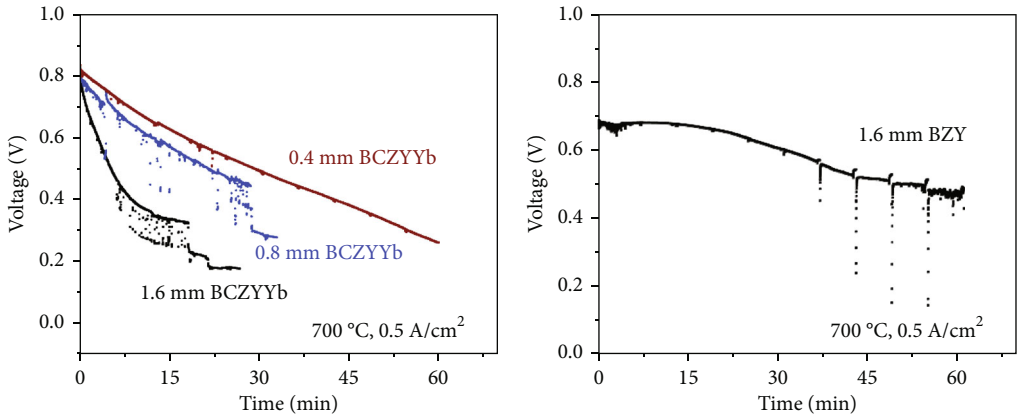

Figure 2: Stability test of (a) BCZYYb and (b) BZY single cells with varying anode thicknesses (1.6, 0.8, and 0.4 mm) during galvanostatic operation at a constant current of 0.5 A/cm^2. The cell voltage is shown as a function of time, and syngas (50% H_2+50% CO) and flowing air were used as the fuel and oxidant, respectively, at 700°C.

of the electrolyte and anode for BCZYYb cells were drastically altered when syngas was used.

To investigate the effect of syngas on the electrochemical performance of the single cells, stability tests were performed with cells fabricated from the two different PC oxides at various anode thicknesses. The anode thickness of the fabricated cell has been characterized by SEM (Figure S2). Figure 2 shows the cell voltage versus time in galvanostatic mode at a constant current of 0.5 A/cm^2 when syngas was the fuel. For the BCZYYb cells, the operation depended on the anode thickness. Increasing the anode thickness induced significantly more rapid degradation, and cell failure occurred within 30 min when the anode thickness was greater than 0.4 mm. A direct comparison between BCZYYb and BZY cells with an anode thickness of 1.6 mm confirmed that the BZY cells degraded more gradually than the BCZYYb cells with rates of 0.24 and 1.2 V/h, respectively.

To study the impact of the catalytic reaction products of the H_2–CO mixture on the cermet anode, the degradation process was carried out under OCV conditions. In this state, the fabricated cells could be considered a pure chemical reactor without any electrochemical reaction. The I–V–P curves and EIS at OCV were collected in 10 and 30 min intervals for BCZYY and BZY cells, respectively, fueled by syngas to confirm the dominant factor of cell degradation. Figures 3(a) and 3(b) illustrate representative I–V–P curves of a BCZYYb cell with a 0.4 mm thick anode and BZY cell with a 1.6 mm thick anode, respectively, as functions of time. Both cells exhibited similar tendencies for the I–V–P curves, where the MPD decreased with increasing time. However, the BCZYYb cells showed a more significant reduction in MPD from the initial value of 0.92 to 0.265 W/cm^2 after 30 min. In contrast, the BZY cells showed a significantly less pronounced decrease from 0.39 to 0.32 W/cm^2 after 1 h. As in the stability test, a similar correlation between the anode thickness and cell degradation was observed; a thinner anode resulted in a more gradual reduction in MPD for the BCZYYb cells (Table 1). This indicates that the observed degradation in the stability test in galvanostatic mode was more likely due to the syngas rather than the applied voltage.

Figures 3(c) and 3(d) show the time-dependent impedance data (R_o and R_p) collected from the fabricated anode-supported BCZYYb and BZY cells at OCV when fueled by syngas. Corresponding Nyquist plot of BCZYYb-based SOFCs with the 0.4 mm and 1.6 mm thick anode as a function of time at OCV at 700°C in syngas fuel is provided in Figure S1. The initial values of R_o for the BCZYYb cells were 0.145, 0.15, and 0.15 Ω·cm^2 with 1.6, 0.8, and 0.4 mm thick anodes, respectively, while the corresponding R_p values were 0.155, 0.1, and 0.08 Ω·cm^2, respectively. Instant increases in R_p and R_o were observed when the balance gas was switched from N_2 to CO, and more rapid degradation was observed with thicker anodes. Thus, the differences in the initial EIS values may be attributed to the sensitivity of the BCZYYb anode to the syngas poisoning effect.

All BCZYYb cells with various anode thicknesses exhibited a <2-fold increase in R_o and >3-fold increase in R_p, even in 30 min. In contrast, the BZY cells showed increases of <10% in 1 h. For example, R_o and R_p were 0.27 and 0.64 Ω·cm^2, respectively, after 30 min for BCZYYb cells with a 1.6 mm thick anode. In contrast, BZY with a corresponding anode thickness had R_o and R_p of 0.34 and 0.11 Ω·cm^2, respectively. In particular, for the BCZYYb cells, a more drastic increase was observed in R_p than in R_o over time, which implies that the degradation of the cell performance with syngas can mainly be attributed to the degradation of the cermet anode. The change in R_p with the anode thickness indicates that reducing the anode thickness will mitigate the degradation, which agrees with the results of the stability test shown in Figure 2.

XRD measurements were conducted with crushed anode powders tested in H_2 and CO+H_2 to investigate the phase decomposition of the anode when fueled by syngas (Figure 4). The fabricated cells were reduced in H_2 at 700°C to obtain the metallic Ni phase, which was followed

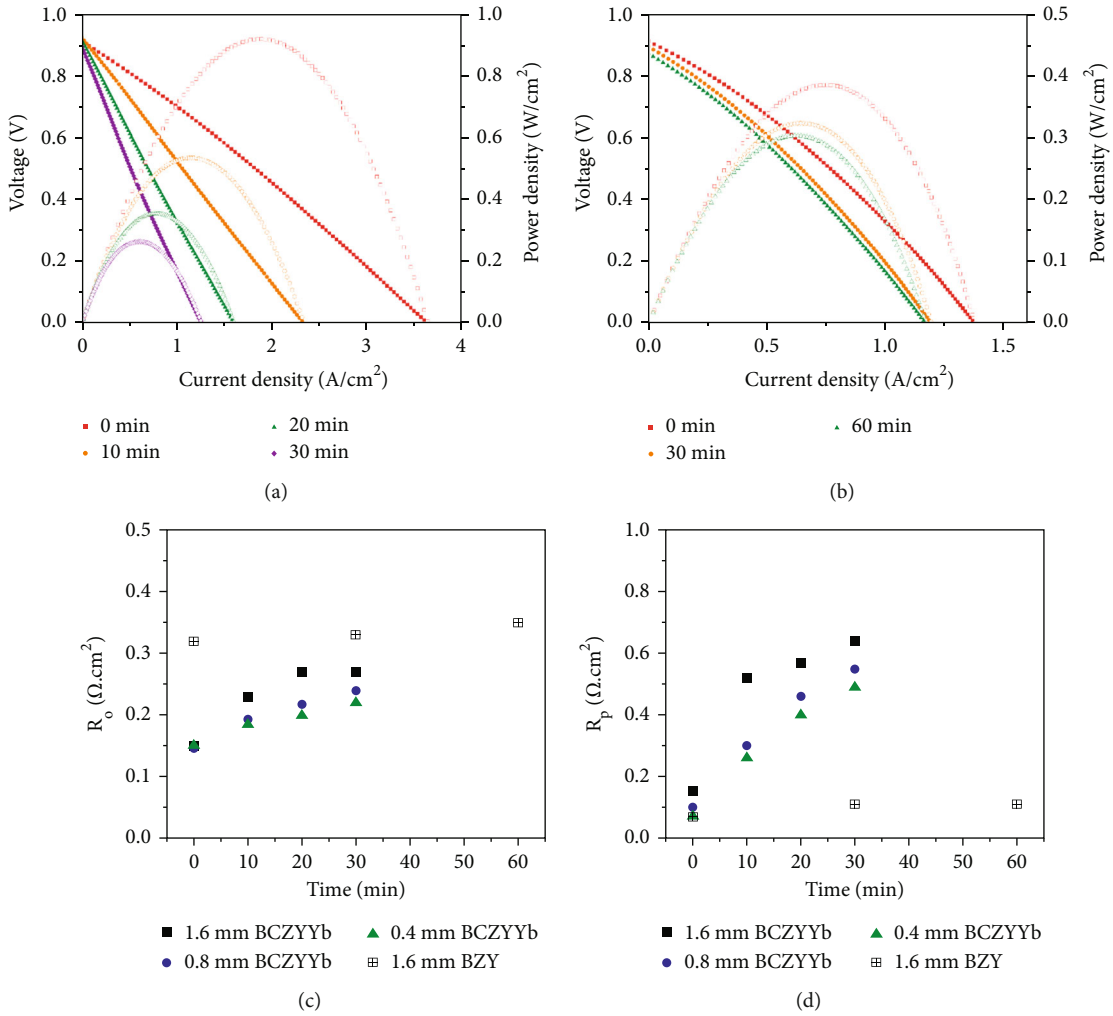

Figure 3: I–V–P curves of (a) BCZYYb and (b) BZY single cells with 0.4 and 1.6 mm thick anodes, respectively, as a function of time at 700°C. Syngas (50% H_2+50% CO) and flowing air were used as the fuel and oxidant, respectively. Time-dependent electrochemical performances of the BCZYYb and BZY single cells: (c) ohmic resistance and (d) polarization resistance at OCV and 700°C.

Table 1: Performances of the BCZYYb and BZY PC-SOFCs at 700°C.

Electrolyte	Electrode	Sintering condition	0 min in syngas			30 min in syngas		
			R_o (Ω·cm^2)	R_p (Ω·cm^2)	MPD (W/cm^2)	R_o (Ω·cm^2)	R_p (Ω·cm^2)	MPD (W/cm^2)
BCZYYb	Ni-BCZYYb 1.6 mm	1400°C 10 h	0.145	0.155	0.743	0.27	0.64	0.14
	Ni-BCZYYb 0.8 mm		0.15	0.1	0.76	0.24	0.57	0.18
	Ni-BCZYYb 0.4 mm		0.15	0.08	0.92	0.236	0.476	0.265
BZY	Ni-BZY 1.6 mm	1450°C 10 h	0.32	0.075	0.39	0.34	0.11	0.32

by exposure to syngas for 1 h. Then, the cells were crushed to obtain the powder samples. After the reduction, the XRD patterns of the BCZYYb-NiO and BZY-NiO anode powders revealed only metallic Ni and perovskite oxide phases, which indicated the complete reduction of NiO and no decomposition of the PC oxide. The XRD patterns of the BCZYYb powder samples clearly showed $BaCO_3$ and doped CeO_2, which confirmed the decomposition by CO_2. The poor chemical stability of ceria-based proton-conducting oxide under CO_2 atmosphere has been reported in the literature [22]. In contrast, NiO-BZY only revealed perovskite oxide and metallic Ni, which indicates that the crystal structure of BZY remained unchanged. The PC oxides utilized in this study (i.e., BCZYYb and BZY) have already been confirmed

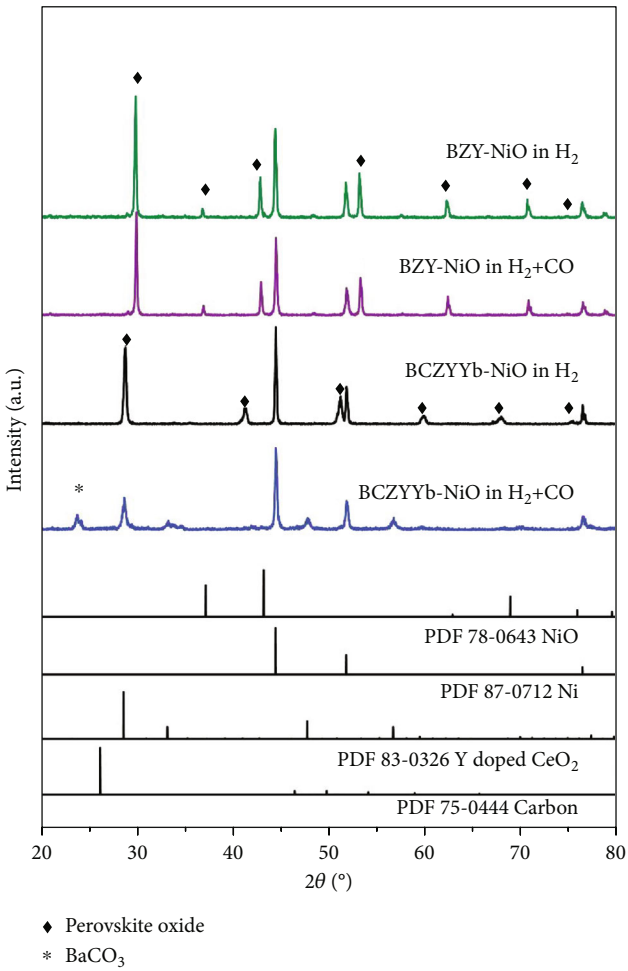

Figure 4: XRD patterns of BCZYYb and BZY anodes powder after 1 h exposure to H_2 and H_2+CO at 700°C.

as chemically stable in H_2 and H_2-CO [23]. However, there is an ongoing discrepancy regarding the stability of BCZYYb in CO_2-containing atmosphere [23–25]. In addition, Hua et al. demonstrated the potential of using PC-SOFCs in syngas fuel stream by the absence of negative effects of CO on electrochemical performance [23], while Sun et al. reported that the Ni-BCZYYb cermet anode was poisoned by extremely low percentage level of CO_2, supporting our observation.

The catalytic reaction of the CO–H_2 mixture was conducted with two different anode powders having 60 wt% NiO, which are denoted as NiO-BCZYYb and NiO-BZY. Figure 5 shows the CO conversion and selectivity to CO_2 and CH_4 as a function of time. The sample sizes of the two different anode powders were varied to study the influence of the residence time. Note that the calculated conversion and selectivity reported in the figures are for gas-phase products only and do not account for carbonaceous deposits. The gas-phase selectivity to the product was defined as the molar ratio of the product to CO+2CO_2+CH_4. All anode powder samples (i.e., NiO-BCZYYb and NiO-BZY) showed similar tendencies for the CO conversion and selectivity to CO_2 and CH_4. The CO conversion and selectivity to CO_2 both showed a gradual increase after an initial rapid decrease. The selectivity to CH_4 showed a rapid decrease. The analogous trends for NiO-BCZYYb and NiO-BZY imply that the catalytic reaction of the CO–H_2 mixture was most likely initiated on the Ni surface, which is supported by the results of Shin et al. [26]. They found that hydrogen dissociation primarily took place on the metallic component of a cermet anode in a pulsed isotope experiment. Increasing the residence time significantly increased the CO conversion and selectivity to CO_2 and CH_4. However, this may be attributed to the increased catalyst bed size.

Interestingly, the selectivity to CO_2 revealed a similar trend to that of the CO conversion for both anode powder samples: a slight decrease in the initial 20 min, which follows the observations for CH_4. This observation was also reported in the literature [27], which indicates that the methanation of CO depends on the extent of deposited carbonaceous species over the metal surface (Equation (1)). The occurrence of the Boudouard reaction (Equation (2)) in the CO–H_2 mixture was evidenced by the formation of CO_2, which deposited carbon over the anode powder surface. Yan et al. reported that CO has no influence on the adsorption of H_2 based on their work with a CO/H_2 competitive adsorption model [19]. Therefore, the deposited carbon may react with dissociated hydrogen over Ni for methanation (Equation (5)). Meanwhile, the continuation of the reaction would lead to the deactivation of Ni catalysts by deposited carbon originating from CO disproportionation, which would block active sites for H_2 adsorption. This hypothesis could be indirectly supported by the rapid reduction of the selectivity to CH_4 over time and also slow deactivation of BZY cells even without phase decomposition. Despite the deactivation of the anode powder in the initial 20 min, the CO conversion and selectivity to CO_2 then gradually increased over time. In addition, a delayed deactivation of CO conversion and selectivity to CO_2 and CH_4 were initially observed for NiO-BZY. This observed delay in deactivation may have been due to the high H_2O uptake capacity of BZY, where the surface hydroxyl compounds can remove adsorbed carbon on Ni [28]. In the present study, no water was utilized; the formation of CH_4 confirmed the occurrence of methanation (Equation (2)), which formed water as a product. Furthermore, in contrast to the delayed deactivation observed for NiO-BZY, NiO-BCZYYb exhibited a higher CO conversion and selectivity to CO_2 after the initial deactivation. The continuous increase in CO conversion and selectivity to CO_2 after the initial deactivation may be attributed to the transition of active sites for CO disproportionation from the metallic Ni to the oxide surface [4]. Furthermore, the higher CO conversion and selectivity to CO_2 for NiO-BCZYYb compared to NiO-BZY after the initial deactivation may be attributed to the enhanced catalytic activity of a new oxide phase, such as doped ceria generated from the decomposition of the perovskite oxide (Figure 4) [4].

$$2CO \longrightarrow CO_2 + C \quad (3)$$

$$3H_2 + CO \longrightarrow CH_4 + H_2O \quad (4)$$

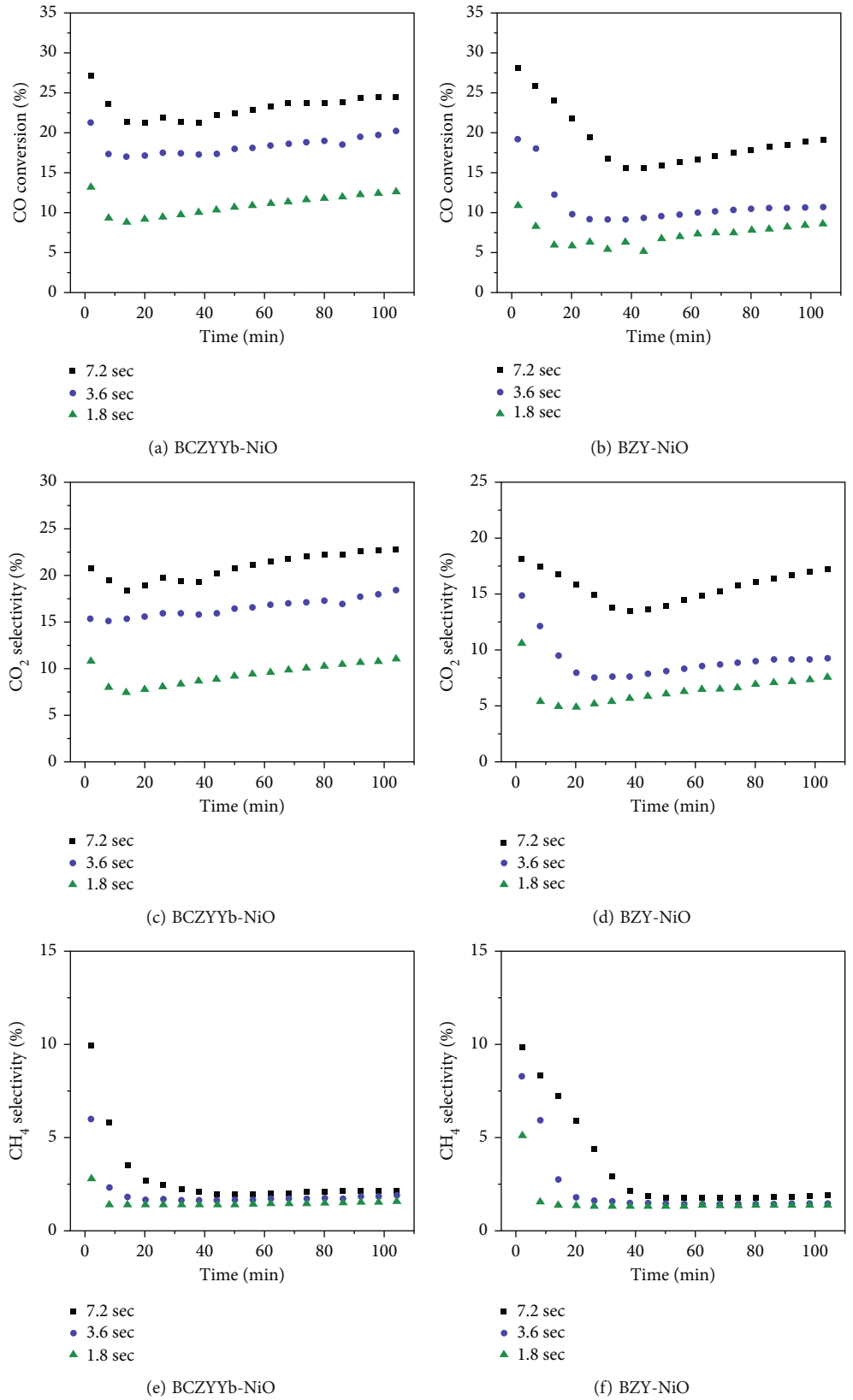

Figure 5: (a, b) CO conversion and selectivity to (c, d) CO_2 and (e, f) CH_4 from the reaction mixture of CO and H_2 versus time when streamed over BCZYYb and BZY anode powders at 700°C and different residence times: 1.8, 3.6, and 7.2 s.

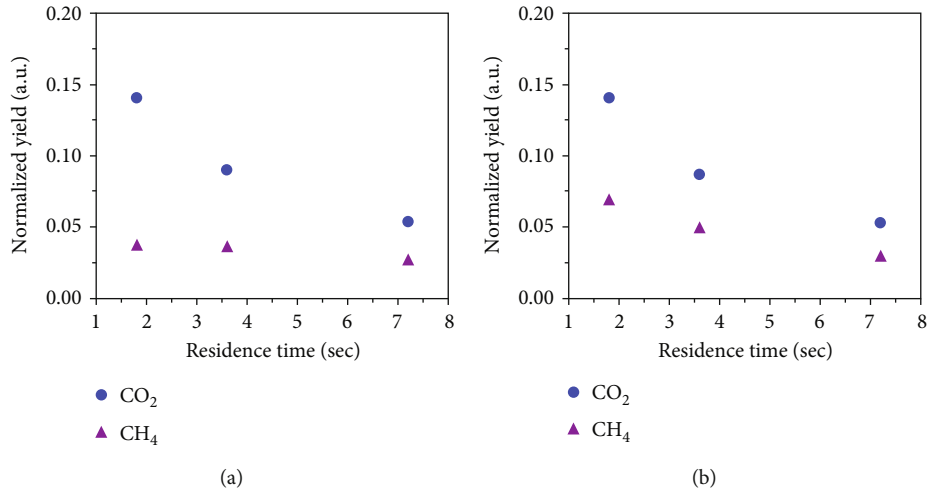

Figure 6: Normalized CO_2 and CH_4 yields at 700°C over (a) BCZYYb and (b) BZY anode powders as a function of residence time.

$$C + 2H_2 \longrightarrow CH_4 \quad (5)$$

Figure 6 shows the influence of the residence time on the CO_2 and CH_4 yields normalized by the mass of the loaded anode powder at 2 min on stream and 700°C. Increasing the residence time significantly decreased the normalized CO_2 yield while having no significant effect on CH_4, which clearly indicates a secondary reaction with the product CO_2. The significantly smaller reduction in the normalized CH_4 yield suggests that the resulting CO_2 was unlikely to be consumed for dry reforming, while it is not clear which reaction pathway prevailed for the secondary reaction of CO_2 because of the complex reaction network [29]. However, the observation of $BaCO_3$ in the BCZYYb anode powder treated in syngas implies that the resulting CO_2 reacted with BCZYYb. Thus, the secondary reaction of CO_2 with BCZYYb may have also contributed to the reduction in the normalized CO_2 yield with increasing residence time, which would further support the more rapid degradation of BCZYYb cells with increasing anode thickness.

4. Conclusion

The present study clearly demonstrated that the electrochemical performance of a syngas-fueled PC-SOFC indeed depends on the PC oxide and anode thickness. This may be correlated with the residence time of the resulting product generated via the catalytic reaction of the H_2–CO mixture in the microporous Ni-based anode. While CO is known to be an inert gas during the operation of PC-SOFCs, the presence of Ni in the anode clearly led to unfavorable side reactions such as CO disproportionation and methanation, which generated carbon coking over the metallic Ni surface and gas-phase CO_2 and CH_4 as products. Thus, it might be carefully suggested to utilize water in syngas fuel stream, or perovskite anode might be a solution to mitigate the carbon coking phenomena in the anode. The resulting gas-phase products may have caused further decomposition of the electrolyte materials in the cermet anode according to the residence time of the reactant in the microporous anode, which is correlated with the anode thickness. The catalytic reaction of the CO–H_2 mixture is hypothesized to primarily take place on the metallic Ni surface. In addition, the less pronounced degradation observed in the BZY cells, despite the unchanged XRD pattern after treatment in syngas, is likely due to carbon coking via CO disproportionation or methanation. Further work is required to understand the exact nature of the active sites for the catalytic reaction of the CO–H_2 mixture and to characterize the deposited carbon on the Ni surface.

Abbreviations

PC-SOFCs: Proton-conducting solid oxide fuel cells
BCZYYb: $BaCe_{0.7}Zr_{0.1}Y_{0.1}Yb_{0.1}O_{3-\delta}$
BZY: $BaZr_{0.8}Y_{0.2}O_{3-\delta}$
PBSCF: $PrBa_{0.5}Sr_{0.5}Co_{1.5}Fe_{0.5}O_{3-\delta}$
AFL: Anode functional layer
MPD: Maximum power density
OCV: Open-circuit voltage
XRD: X-ray diffraction
SEM: Scanning electron microscopy
TCD: Thermal conductivity detector
R_o: Ohmic resistance
R_p: Polarization resistance.

Data Availability

Crystallographic data for the structures reported in this manuscript have been deposited with MDI JADE software. Copies of these data can be obtained from http://www.ccdc.cam.ac.uk.

Conflicts of Interest

There are no conflicts to declare.

Acknowledgments

This research was supported by the Basic Science Research Program through National Research Foundation of Korea (NRF) funded by the Ministry of Education, South Korea (no. NRF2021R1I1A1A01057519), the National Research Foundation of Korea (NRF) grant funded by the Korea government (MSIT) (NRF2021R1A5A1084921 and NRF2021M3H4A1A02055684), and the Korea Institute of Energy Technology Evaluation and Planning (KETEP) grant funded by the Korea government (MOTIE) (no. 20212010100040).

Supplementary Materials

Figure S1 shows the Nyquist plot of BCZYYb-based SOFCs with the 0.4 mm and 1.6 mm thick anode as a function of time at OCV at 700°C in syngas fuel, indicating that thicker anode results in more significant increase of R_p. Figure S2 is the SEM image of anode-supported PC-SOFC fabricated with different anode thicknesses: (a, b) 1.6 mm, (c, d) 0.8 mm, and (e, f) 0.4 mm. *(Supplementary Materials)*

References

[1] T. Raza, J. Yang, R. Wang et al., "Recent advance in physical description and material development for single component SOFC: a mini-review," *Chemical Engineering Journal*, vol. 444, article 136533, 2022.

[2] M. Liu, M. E. Lynch, K. Blinn, F. M. Alamgir, and Y. Choi, "Rational SOFC material design: new advances and tools," *Materials Today*, vol. 14, no. 11, pp. 534–546, 2011.

[3] S. McIntosh and R. J. Gorte, "Direct hydrocarbon solid oxide fuel cells," *Chemical Reviews*, vol. 104, no. 10, pp. 4845–4866, 2004.

[4] M. Kogler, E. M. Köck, B. Klötzer et al., "High-temperature carbon deposition on oxide surfaces by CO disproportionation," *Journal of Physical Chemistry C*, vol. 120, no. 3, pp. 1795–1807, 2016.

[5] J. H. Shim, "Ceramics breakthrough," *Nature Energy*, vol. 3, no. 3, pp. 168-169, 2018.

[6] T. Norby, "Solid-state protonic conductors: principles, properties, progress and prospects," *Solid State Ionics*, vol. 125, no. 1-4, pp. 1–11, 1999.

[7] S. Choi, C. J. Kucharczyk, Y. Liang et al., "Exceptional power density and stability at intermediate temperatures in protonic ceramic fuel cells," *Nature Energy*, vol. 3, no. 3, pp. 202–210, 2018.

[8] C. Duan, J. Tong, M. Shang et al., "Readily processed protonic ceramic fuel cells with high performance at low temperatures," *Science*, vol. 349, pp. 1321–1326, 2015.

[9] S. Sun, O. Awadallah, and Z. Cheng, "Poisoning of Ni-based anode for proton conducting SOFC by H_2S, CO_2, and H_2O as fuel contaminants," *Journal of Power Sources*, vol. 378, pp. 255–263, 2018.

[10] L. Wang, Y. Fan, J. Li et al., "$La_{0.5}Sr_{0.5}Fe_{0.9}Mo_{0.1}O_{3-\delta}$-$CeO_2$ anode catalyst for Co-producing electricity and ethylene from ethane in proton-conducting solid oxide fuel cells," *Ceramics International*, vol. 47, no. 17, pp. 24106–24114, 2021.

[11] Y. Wang, X. Lei, Y. Zhang, F. Chen, and T. Liu, "In-situ growth of metallic nanoparticles on perovskite parent as a hydrogen electrode for solid oxide cells," *Journal of Power Sources*, vol. 405, pp. 114–123, 2018.

[12] N. Yu, T. Liu, X. Chen, M. Miao, M. Ni, and Y. Wang, "Co-generation of liquid chemicals and electricity over Co-Fe alloy/perovskite anode catalyst in a propane fueled solid oxide fuel cell," *Separation and Purification Technology*, vol. 291, article 120890, 2022.

[13] B. Hua, M. Li, J. L. Luo, J. Pu, B. Chi, and J. Li, "Carbon-resistant Ni-$Zr_{0.92}Y_{0.08}O_{2-\delta}$ supported solid oxide fuel cells using Ni-Cu-Fe alloy cermet as on-cell reforming catalyst and mixed methane-steam as fuel," *Journal of Power Sources*, vol. 303, pp. 340–346, 2016.

[14] T. Wei, P. Qiu, L. Jia et al., "Power and carbon monoxide co-production by a proton-conducting solid oxide fuel cell with $La_{0.6}Sr_{0.2}Cr_{0.85}Ni_{0.15}O_{3-\delta}$for on-cell dry reforming of CH4by CO2," *Journal of Materials Chemistry A*, vol. 8, no. 19, pp. 9806–9812, 2020.

[15] P. Schwach, X. Pan, and X. Bao, "Direct conversion of methane to value-added chemicals over heterogeneous catalysts: challenges and prospects," *Chemical Reviews*, vol. 117, no. 13, pp. 8497–8520, 2017.

[16] M. Li, B. Hua, and J. L. Luo, "Alternative fuel cell technologies for cogenerating electrical power and syngas from greenhouse gases," *ACS Energy Letters*, vol. 2, no. 8, pp. 1789–1796, 2017.

[17] T. Wan, A. Zhu, Y. Guo et al., "Co-generation of electricity and syngas on proton-conducting solid oxide fuel cell with a perovskite layer as a precursor of a highly efficient reforming catalyst," *Journal of Power Sources*, vol. 348, pp. 9–15, 2017.

[18] O. Costa-Nunes, R. J. Gorte, and J. M. Vohs, "Comparison of the performance of Cu–CeO_2–YSZ and Ni–YSZ composite SOFC anodes with H_2, CO, and syngas," *Journal of Power Sources*, vol. 141, no. 2, pp. 241–249, 2005.

[19] N. Yan, X. Z. Fu, K. T. Chuang, and J. L. Luo, "Insights into CO poisoning in high performance proton-conducting solid oxide fuel cells," *Journal of Power Sources*, vol. 254, pp. 48–54, 2014.

[20] C. Lee, S. S. Shin, J. Kim et al., "Tailoring an interface microstructure for high-performance reversible protonic ceramic electrochemical cells via soft lithography," *ACS Applied Materials & Interfaces*, vol. 14, no. 28, pp. 32124–32133, 2022.

[21] Y. Jiang and A. V. Virkar, "Fuel composition and diluent effect on gas transport and performance of anode-supported SOFCs," *Journal of the Electrochemical Society*, vol. 150, no. 7, article A942, 2003.

[22] E. Fabbri, D. Pergolesi, A. D'Epifanio et al., "Design and fabrication of a chemically-stable proton conductor bilayer electrolyte for intermediate temperature solid oxide fuel cells (IT-SOFCs)," *Energy & Environmental Science*, vol. 1, no. 3, pp. 355–359, 2008.

[23] B. Hua, N. Yan, M. Li et al., "Novel layered solid oxide fuel cells with multiple-twinned $Ni_{0.8}Co_{0.2}$ nanoparticles: the key to thermally independent CO_2 utilization and power-chemical cogeneration," *Energy & Environmental Science*, vol. 9, no. 1, pp. 207–215, 2016.

[24] C. Zuo, S. Zha, M. Liu, M. Hatano, and M. Uchiyama, "$Ba(Zr_{0.1}Ce_{0.7}Y_{0.2})O_{3-\delta}$ as an electrolyte for low-temperature solid-oxide fuel cells," *Advanced Materials*, vol. 18, no. 24, pp. 3318–3320, 2006.

[25] S. Fang, K. S. Brinkman, and F. Chen, "Hydrogen permeability and chemical stability of Ni–$BaZr_{0.1}Ce_{0.7}Y_{0.1}Yb_{0.1}O_{3-\delta}$ membrane in concentrated H_2O and CO_2," *Journal of Membrane Science*, vol. 467, pp. 85–92, 2014.

[26] H. H. Shin and S. McIntosh, "On the H_2/D_2 isotopic exchange rate of proton conducting barium cerates and zirconates," *Journal of Materials Chemistry A*, vol. 1, no. 26, pp. 7639–7647, 2013.

[27] M. Araki and V. Ponec, "Methanation of carbon monoxide on nickel and nickel-copper alloys," *Journal of Catalysis*, vol. 44, no. 3, pp. 439–448, 1976.

[28] C. Duan, R. J. Kee, H. Zhu et al., "Highly durable, coking and sulfur tolerant, fuel-flexible protonic ceramic fuel cells," *Nature*, vol. 557, no. 7704, pp. 217–222, 2018.

[29] G. B. Johnson, P. Hjalmarsson, K. Norrman, U. S. Ozkan, and A. Hagen, "Biogas catalytic reforming studies on nickel-based solid oxide fuel cell anodes," *Fuel Cells*, vol. 16, no. 2, pp. 219–234, 2016.